# Passive Guidance Forces of Polarized Linear Motors Combined With Levitation Actuators Working in Partial Vacuum – Application to Swissmetro

[1]CASSAT Alain, [2]ESPANET Christophe, [3]BOURQUIN Vincent, [4]JUFER Marcel, [5]PEREY Raphael

[1, 4]*Ecole Polytechnique Fédérale de Lausanne, Laboratory of Integrated Actuators*
*CH-1015 Lausanne, Switzerland*
[1]*Phone: (++41) 21 693 26 91; Fax: (++41) 21 693 26 87; E-mail :alain.cassat@epfl.ch*
[3]*Phone: (++41) 21 693 70 51; Fax: (++41) 21 693 26 87; E-mail: marcel.jufer@epfl.ch*

[2]*University of Franche-Comté, Laboratory of Research in Electrical Engineering and Systems*
*L2ES/UTBM, bât. F, rue Ernest Thierry-Mieg, F-90010-Belfort Cedex, France*
*Phone: (++33) 3 84 58 36 14; Fax: (++33) 3 84 58 36 36; E-mail: christophe.espanet@univ-fcomte.fr*

[3, 5]*Numexia, EPFL-PSE-A, CH-1015 Lausanne, Switzerland*
*Phone: (++41) 21 693 87 37; E-mail:vincent.bourquin@numexia.com*

ABSTRACT: Maglev (>400 km/h) refer to Maglev such as the Japanese JR-Maglev MLX, the German Transrapid and the USA Inductrack. The Swissmetro Project, presenting a unique aspect of Maglev, is designed to work under partial vacuum (<10 kPa) in two tunnels and for high speeds (>400 km/h). The authors investigate the combination of the propulsion with the levitation. To minimize the heat due to the iron and copper losses, a polarized excitation is proposed with NdFeB PM for the magnetic way poles. This paper emphasis the determination of the passive guidance forces of the active magnetic way, based on 3D FEM analysis. The possibility, to use these passive forces to guide the vehicle, is presented. This paper describes the issues related to such technical choices.

## 1 INTRODUCTION

For high speed Maglev[1 to 7], only linear synchronous motors are considered for the propulsion. Swissmetro is a Maglev Project[8, 9], designed for speeds up to 500 km/h in two tunnels of 5 m inside diameter, under a partial vacuum of 8000 Pa. For long stators fixed with the tunnel, the authors propose new combinations of the electromechanical functions[10 to 12] (see Chapter Specifications, Variant D), such as the propulsion is combined with the levitation working by attraction. Such an approach is still not applied for high speed Maglev, requiring mechanical power higher than 6 MW, but only appears in Urban Rapid Transit Maglev (< 160 km/h). The motor magnetic way uses NdFeB permanent magnets for the excitation. The objectives of these combinations are the following:

- to decrease heat (copper losses) in the levitation and guidance inductors;
- to decrease the number of the reference surfaces, for which the air gap is specified. An air gap of 20 mm is specified for the propulsion, the levitation and the guidance.

For the guidance, there is a clear interest to investigate the possibility to use the passive guidance forces produced by the motors in order to guide transversally the vehicle.

Both the polarization of the levitation inductors and the passive guidance of the vehicle are actually not considered for high speed Maglev. This paper presents the corresponding design key points.

The propulsion and the magnetic levitation were investigated in References [10, 11, 12]. In this paper, the corresponding Chapters 3 and 4 give only the key results for the propulsion and the levitation.

## 2 MAIN SPECIFICATIONS

### 2.1 Propulsion

The total mechanical power is 6 MW. The magnetic ways are distributed, on both vehicle sides, in the nose, the four vehicle cells and the trail. Each active part of the motors sees a twelfth of the total propulsion force and of the total mechanical power.

## 2.2 Vehicle in a Curve

The specification concerning the levitation and the guidance are given, with respect to Figure 1.
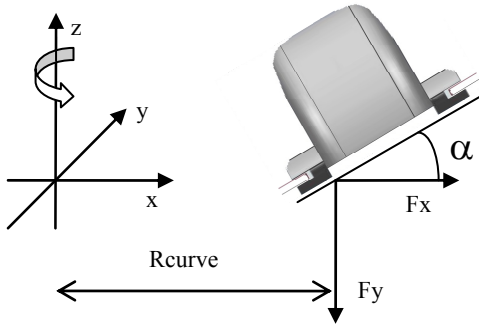


Figure 1: Vehicle in a curve of inclination α, vehicle moving in direction y

The forces Fx and Fy are defined as follows:

$$Fx = m_{total} \cdot \frac{v_y{}^2}{R_{curve}} \qquad [N] \quad (1)$$

$$Fy = m_{total} \cdot g \qquad [N] \quad (2)$$

## 2.3 Levitation

Figure 1 gives the conditions that the vehicle has to satisfy for the levitation. The levitation force is expressed as:

$$F_{levitation} = Fx \cdot \sin(\alpha) + Fy \cdot \cos(\alpha) \qquad [N] \quad (3)$$

## 2.4 Guidance

Figure 1 gives the conditions that the vehicle has to satisfy for the guidance. The guidance force is expressed as:

$$F_{guidance} = Fx \cdot \cos(\alpha) - Fy \cdot \sin(\alpha) \qquad [N] \quad (4)$$

### 2.4.1 Passenger Comfort

The International Standard [ISO 2631] applies to vibrations in both vertical and horizontal directions, dealing with random and shock vibration and harmonic vibration. The passenger comfort imposes a maximum admissible acceleration of 0.8 m/s² for the Swiss Federal Trains. Defining the following RMS comfort acceleration, with T being the period of time over which the acceleration is measured:

$$a_{comfort} = \sqrt{\frac{1}{T}\int_0^T a^2(t) \cdot dt} \qquad [N] \quad (5)$$

For a vehicle in a curve of radius Rcurve and a plane inclination angle α, the following relation defines the maximum vehicle speed $v_y$:

$$a_{comfort} = \frac{v_y{}^2}{R_{curve}} \cdot \cos(\alpha) - g \cdot \sin(\alpha) \qquad [N] \quad (6)$$

The ideal passenger comfort corresponds to a full compensation of the acceleration, such as:

$$0 = \frac{v_y{}^2}{R_{curve}} \cdot \cos(\alpha) - g \cdot \sin(\alpha) \qquad [N] \quad (7)$$

Figure 2 shows the curve radius Rcurve for different admissible accelerations with no curve inclination. Figure 3 gives the curve inclinations, for a speed of 400 km/h and satisfying the passenger acceleration of 0 m/s² (full compensation) and 0.8 m/s² (see Equations 6, 7).
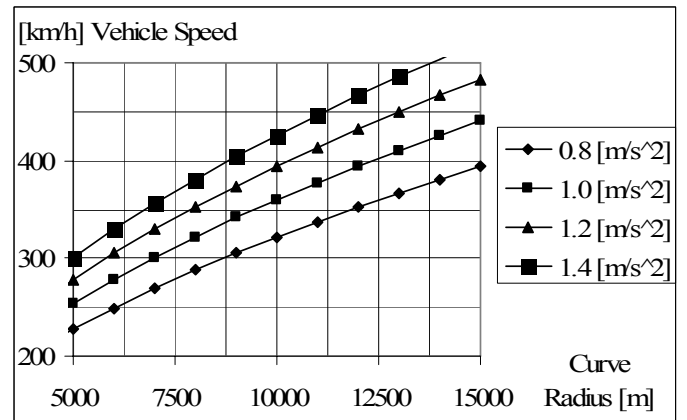


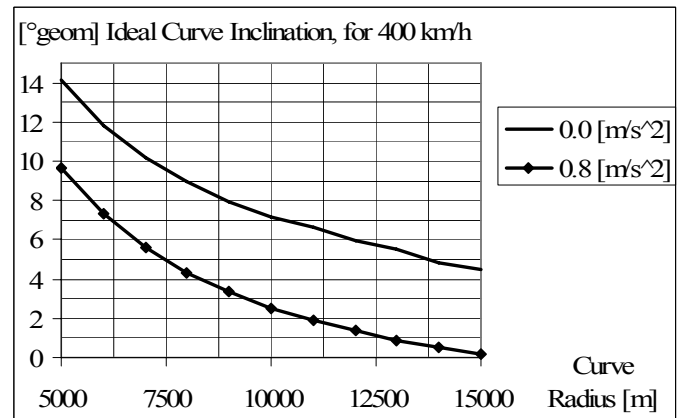Figure 2: Vehicle speed versus curve radius for given accelerations supported by the passengers



Figure 3: Ideal curve inclinations: vehicle speed versus curve radius for given accelerations supported by the passengers

### 2.4.2 Design Cases

The design criteria are determined by the maximum required guidance force. Two cases are considered.

*Case 1 - passenger comfort*: Admitting a maximum admissible acceleration of 0.8 m/s² and a non

total compensation of the acceleration, Equation 8 expresses the total guidance force. The necessary guidance force is equal to 64000 N.

$$F_{guidance} = m_{total} \cdot a_{comfort} = 80000 \cdot 0.8 = 64000 \, [N] \quad (8)$$

*Case 2 - vehicle at stalls*: Figure 1 shows that another limit case is defined when the vehicle stalls, at no speed, in a curve of maximum inclination. For a maximum plane inclination curve of 9.66°, the guidance force becomes:

$$F_{guidance} = m_{total} \cdot g \cdot \sin(\alpha) = 134240 \quad [N] \quad (9)$$

Equation 9 represents the worst case. Chapters 5, 6 describe design strategies to satisfy these two cases.

## 3  PROPULSION

Figure 4 represents the principle of the motor. Only two poles are presented. The stator winding has a fractional number of slots per pole and per phase of 0.364 and a coil opening of one slot. The stator has two coils per slot. For the elementary stator section the number of slots is 24, corresponding to a number of poles of 22.

One pole has a NdFeB permanent magnet MMF of 13.1 kA, for 16×90×231 mm dimensions. The magnets have a remanent flux density of 1.23 T.

In order to decrease the PM iron losses, the permanent magnet poles are segmented in two segments in the active width direction and in eight PM segments in the pole pitch direction. Table 1 gives the power balance of the complete vehicle for a stator sector length of 80 m, corresponding to the vehicle length. Figure 5 shows the efficiency of the system as a function of the stator section length.
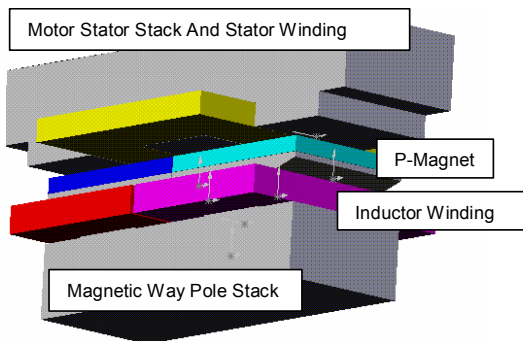


Figure 4: Motor: combined propulsion with levitation

Table 1: Power balance corresponding to a vehicle stator section length of 80 m and a speed of 500 km/h.

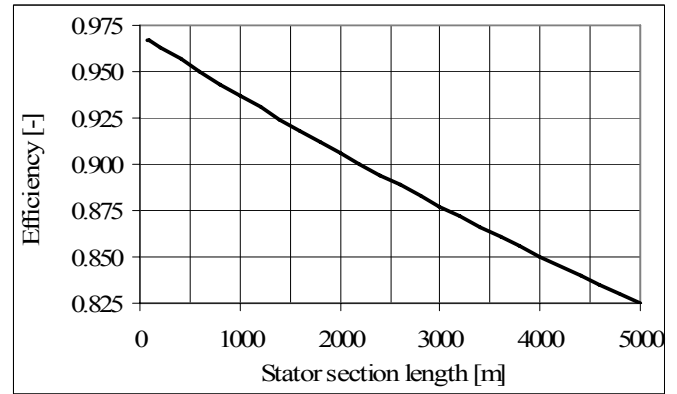| Mech | Stator | | Magnetic way | |
|------|--------|--|--------------|--|
|      | Joule | Iron losses | Yoke | P-magnet |
| 6 [MW] | 17.4 [kW] | 46.2 [kW] | 11.6 [kW] | 128 [kW] |



Figure 5: Efficiency versus the stator section length

## 4  LEVITATION

Figure 6 gives the evolution of the attractive force versus position. Figure 7 shows the evolution of the attractive force versus the compensation MMF of the additional inductor winding.
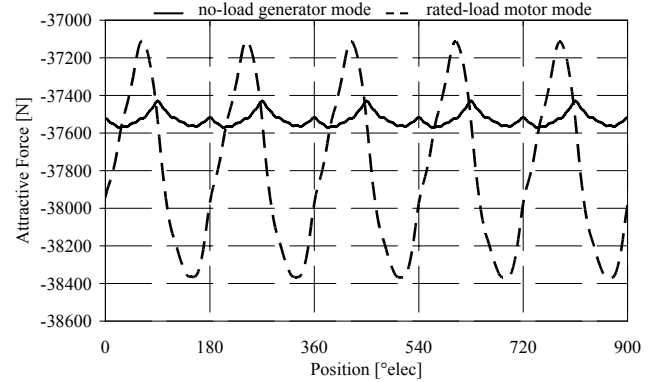


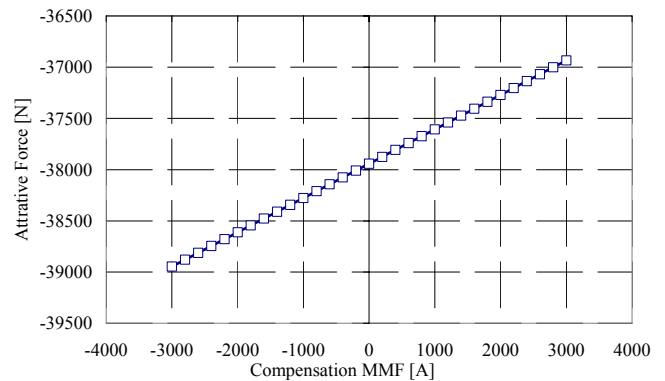Figure 6: Attractive force (PM with 8 segments, 22 poles)



Figure 7: Attractive force versus compensation MMF of the pole inductor (PM with 8 segments, 22 poles)

# 5 PASSIVE GUIDANCE FORCES

## 5.1 Force Components

Figure 8 shows a 3D view and both longitudinal and transverse views of the motor with the corresponding geometrical parameters.

Figure 9 gives the spatial distribution of the flux lines around the air-gap in a transverse plane. It permits to define three zones of magnetic flux: zones 1 and 3 are related to the side fringe fluxes and zone 3 to the main flux.
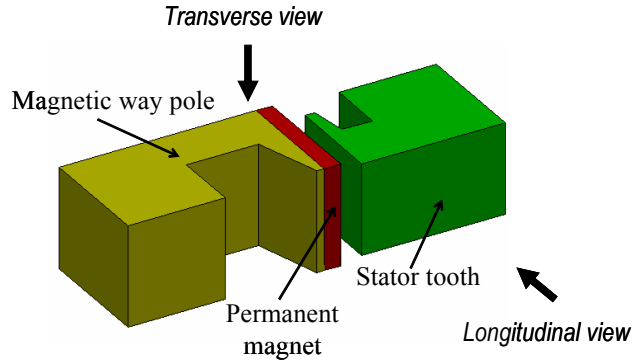


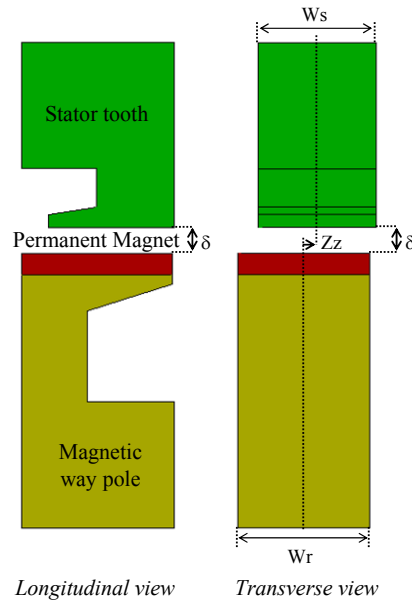Figure 8a: Motor geometry 3D FEM model for guidance force determination



Longitudinal view      Transverse view
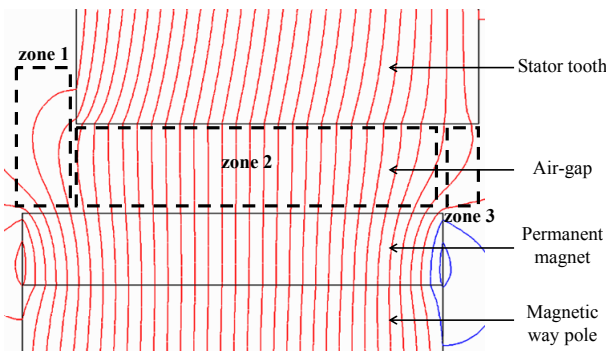
Figure 8b: Motor geometry – longitudinal and transverse views



Figure 9: Air-gap flux line distribution in the transverse plane Case: Wr = 94 mm; Ws = 90 mm; Air gap = 20 mm; Transverse eccentricity Zz = 10 mm

Since 3D FEM investigation is necessary, a first order analysis is presented only to emphases the force components. As shown in Figure 9, for the transverse offset or eccentricity Zz, the passive guidance forces are produced by the variation of the magnetic energy in the air gap zones, such as: the side flux (zones 1 and 3) and the main flux (zone 2). The air gap permeance is expressed, as a function of the transverse offset or eccentricity Zz. Its derivative is defined as follows:

For $0 \leq Zz \leq \dfrac{Wr}{2} - \dfrac{Ws}{2}$, the permeance derivative is:

$$\frac{d\Lambda_\delta}{dZz} = \frac{-\pi \cdot \mu_0 \cdot l_{mot} \cdot Zz}{\left(\delta + \dfrac{\pi}{2} \cdot \left(\dfrac{Wr}{2} - \dfrac{Wr}{2} + Zz\right)\right) \cdot \left(\delta + \dfrac{\pi}{2} \cdot \left(\dfrac{Wr}{2} - \dfrac{Ws}{2} - Zz\right)\right)}$$

(10)

If the flux density is homogeneous, the previous equations indicate that the passive guidance force is mainly produced by the fringe fluxes, resulting of the antagonist forces produced in Zones 1 and 3. Zone 2 does not produce a force.

For $Zz \geq \dfrac{Wr}{2} - \dfrac{Ws}{2}$, the derivative of the air gap permeance is expressed, as follows:

$$\frac{d\Lambda_\delta}{dZz} = \mu_0 \cdot \frac{l_{mot}}{\delta} \qquad [H/m] \quad (11)$$

The transverse force, function of Zz, becomes:

$$F_{Zz} = \frac{1}{2} \cdot \frac{d\Lambda_\delta}{dZz} \cdot \left(\frac{B_\delta \cdot \delta}{\mu_0}\right)^2 \qquad [N] \quad (12)$$

Due to the presence of the PM, the flux lines are not perpendicular to its surface, thus a homogeneous flux density in the air gap cannot be obtained. Furthermore, the fringe effect depends highly on the longitudinal geometries of the magnetic way (poles) and the stator (teeth), as seen in Figure 8b. These geometry effects cannot be easily expressed in the previous equations, but are investigated with a 3D FEM. Consequently the use of Equations 10 to 12, requiring a homogeneous flux density in the air gap, leads to an inaccurate evaluation of the transverse forces. Versus the admissible domain of the transverse eccentricity Zz, these equations clearly indicate that if the flux density is homogeneous then:

- the passive guidance force (transverse force), versus the transverse eccentricity, will be relatively low then very high. Equations 11

and 12 show that a constant force will be produced.

Two design concepts are proposed to increase the passive guidance force. These two concepts, analyzed in the next chapter, are defined as follows:

1. Introduction of a geometry condition such as Wr>Ws, in order to reinforce the homogeneity of the flux density in the air gap;
2. Segmentation of the complete motor in two, in the transverse direction. This is all the most possible since already the PM are segmented in two in the transverse direction as described in Chapter 3.

### 5.2 3D Finite Element Method Simulations

3D FEM simulations permit to investigate these two concepts. The different cases are simulated considering the passive guidance force produced only by the permanent magnet. The influence of the magnetic field created by the stator currents is not considered. Only half stator and magnetic way poles are described, as shown in Figure 8.

First the ratio of the magnetic way width Wr and the stator stack width Ws is investigated. On the surface of calculation defined in Figure 10, the flux density in the air-gap is determined. Figure 11 shows the corresponding results, proving that the homogeneity of the flux density under the stator tooth is improved by increasing the magnetic way width Wr.
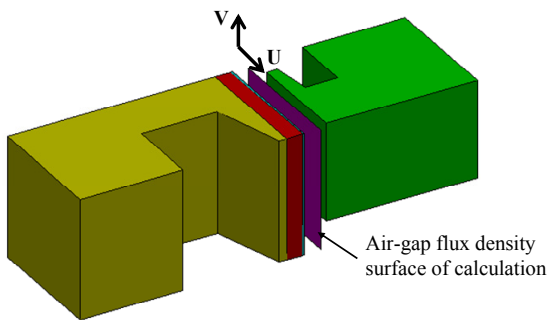


Figure 10: 3D definition of the air-gap flux density surface of calculation

Moreover, the increase of the magnetic way width makes it possible to increase the surface of the permanent magnet which does not see the stator stack width. Consequently, the magnetic flux which is involved in the fringes increases, i.e. the flux component which creates the magnetic passive guidance force. Figure 12 clearly shows it, where the flux lines and the magnetic pressure are plotted.

Due to the high permeability of the stator tooth, the flux lines are nearly purely perpendicular at the surface of the tooth. Then, the tangential component of the Maxwell stress tensor can be neglected in

comparison with the normal one confirming that the major component of the magnetic passive guidance force is related to the lateral surfaces of the tooth, i.e. the fringes. This point is emphases in Figure 13. Figure 13 shows that the force increases when the magnetic way width is increased, the stator width being constant. The considered limit is chosen to be Wr = 112 and Ws = 90 mm, since a further increase of the magnetic way width does not bring anymore a sufficient increase of the passive guidance force.
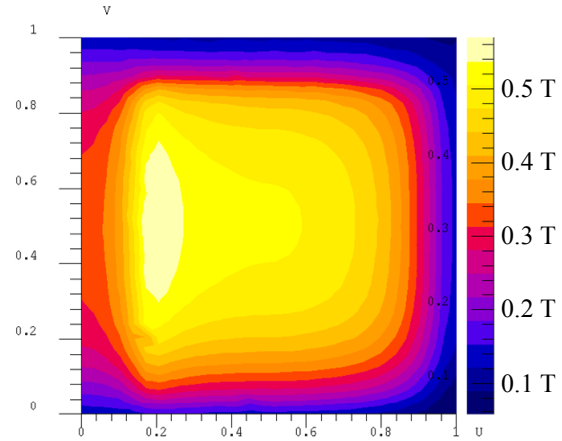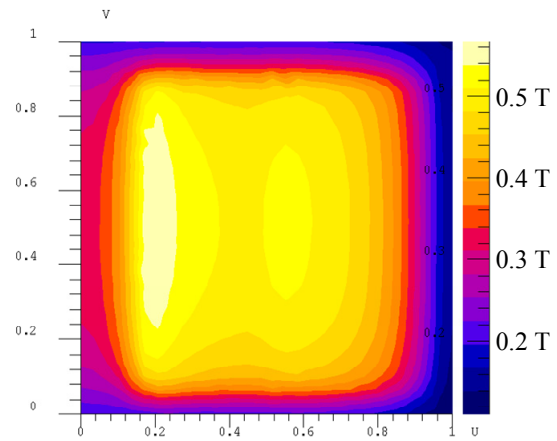


Figure 11: 3D FEM - Color shaded of the air-gap flux density
Case 1: Wr = 94 mm; Ws = 90 mm; Air gap = 20 mm
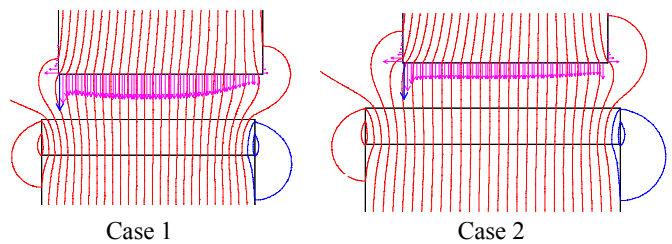Case 2: Wr = 112 mm; Ws = 90 mm; Air gap = 20 mm
Transverse eccentricity Zz = 5.5 mm



Figure 12: 3D FEM - Transverse flux lines in the air-gap and magnetic pressure on the stator tooth surface
Case 1: Wr = 94 mm; Ws = 90 mm; Air gap = 20 mm
Case 2: Wr = 112 mm; Ws = 90 mm; Air gap = 20 mm
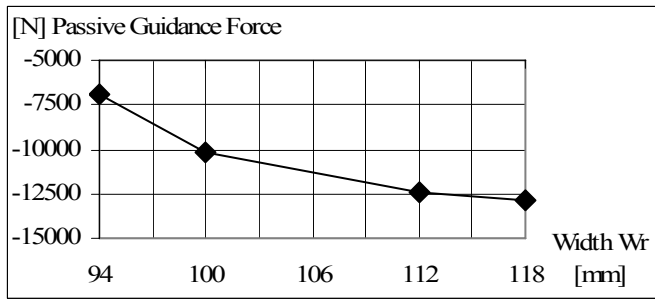Transverse eccentricity Zz = 5.5 mm

Figure 13: Guidance force versus the magnetic way width Wr
Case:  Ws = 90 mm; Air gap = 20 mm;
       Transverse eccentricity Zz = 2 mm

Table 2 presents the 3D FEM simulation cases. In Table 2, Zz1 is the transverse eccentricity satisfying the specified force of -64000 N, Kz the gradient of the transverse force versus the transverse eccentricity, $\acute{\omega}$ the pulsation, T the time period of the elementary oscillator, $a_{max}$ the maximum acceleration, $v_{max}$ the maximum speed, $W_{kinetic}$ the kinetic energy and $P_{max}$ the maximum power. These values are introduced in Chapter 6.

Figure 14 represents the passive guidance forces for the different cases 1 to 4 defined in Table 2.

Table 2: Considered parameter cases for 3D FEM analysis and results (see Fig. 14 and Chapter 6)
Maximum acceleration, energy and maximum power are determined for a variation $\Delta Zz = 5.5$  mm
Zz1 is determined for a transverse force of 64000 N

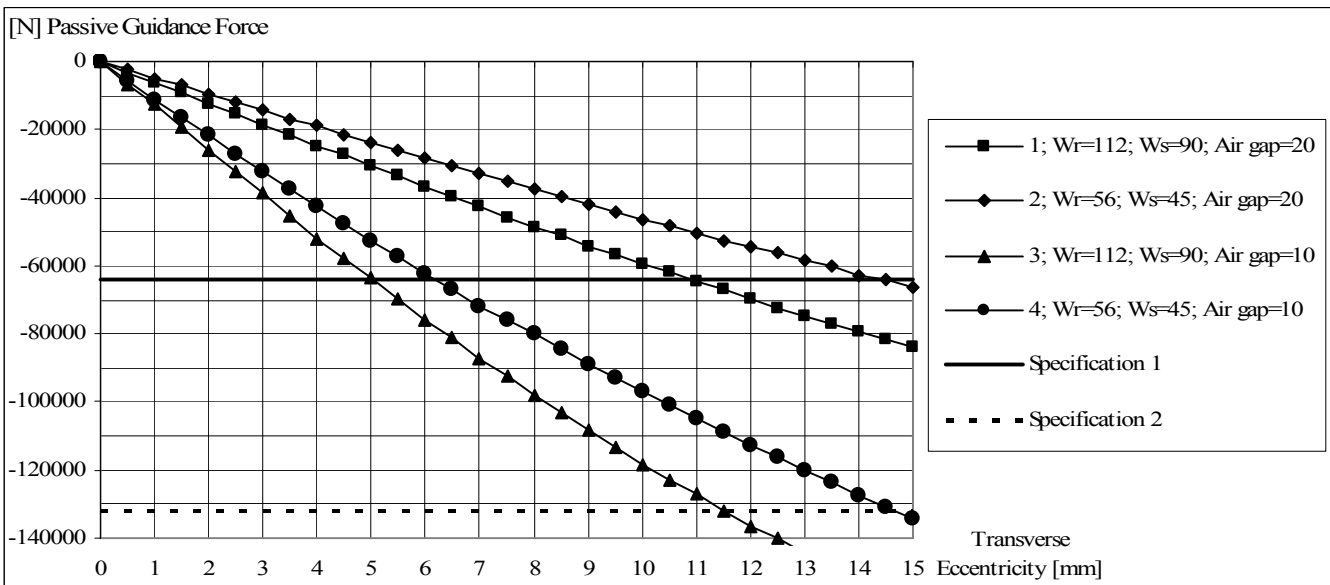| Wr | Ws | Air Gap | Zz1 | Kz | w | T | $a_{max}$ | $v_{max}$ | $W_{kinetic}$ | $P_{max}$ | Fig. 14 |
|----|----|---------|-----|-----|-----|-----|-----------|-----------|---------------|-----------|---------|
| [mm] | [mm] | [mm] | [mm] | [MN/m]] | [1/s] | [s] | [m/s²] | [m/s] | [J] | [W] | Cases |
| 112 | 90 | 20 | 11.0 | -5.88 | 8.570 | 0.7349 | 0.4039 | 0.0471 | 88.86 | 761.49 | 1 |
| 56 | 45 | 20 | 14.5 | -4.44 | 7.451 | 0.8452 | 0.3054 | 0.0410 | 67.18 | 500.56 | 2 |
| 112 | 90 | 10 | 5.0 | -12.74 | 12.621 | 0.4990 | 0.8761 | 0.0694 | 192.74 | 2432.53 | 3 |
| 56 | 45 | 10 | 6.0 | -10.38 | 11.393 | 0.5528 | 0.7139 | 0.0627 | 157.06 | 1789.36 | 4 |



Figure 14: 3D FEM Passive guidance force versus transverse eccentricity; Complete vehicle – stator tooth axis is in the axis of the magnetic way pole transition

## 5.3 Results Analysis

### 5.3.1 Guidance Force Versus The Eccentricity

For the admissible domain of the transverse eccentricity, the passive guidance force appears to be almost a linear force. The force can be expressed as a linear function of the transverse eccentricity. The gradient of the force Kz can be determined.

An investigation of the passive guidance force for a transverse eccentricity above the admissible values is presented in Figure 15. It defines an absolute limit of the eccentricity, which equals to 72 mm: if the eccentricity is higher than this limit, the guidance force will decrease and the system is unstable.
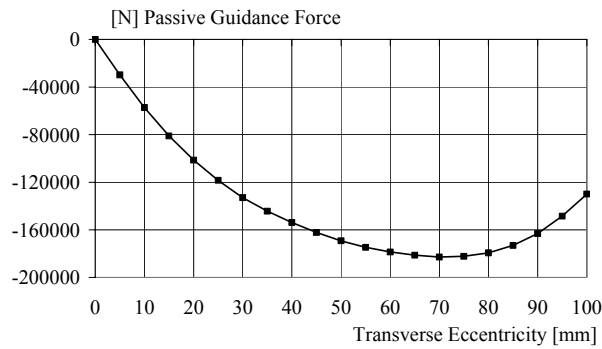


Figure 15: 3D FEM - Passive guidance force versus the transverse eccentricity
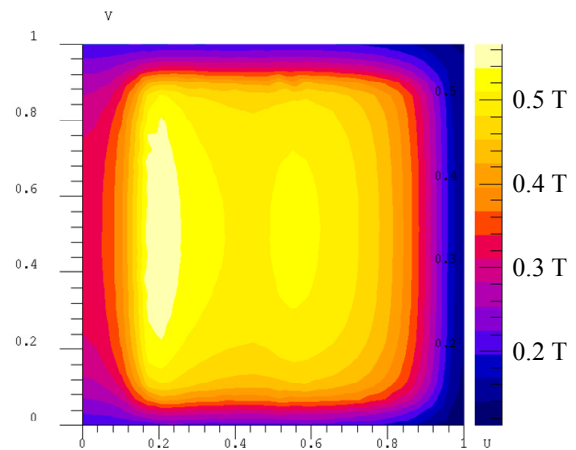Case: Wr = 112 mm; Ws = 90 mm; Air gap = 20 mm

### 5.3.2 Guidance force versus the air-gap

Figure 16 presents the flux density in the air-gap (see surface of calculation in Figure 10) for two values of the air-gap, respectively 20 mm and 10 mm. It clearly shows the two interests of decreasing the air-gap. First the homogeneity of the flux density is improved and second the magnitude of the flux density is increased. These two characteristics imply an increase of the guidance force, as shown in Figure 14.

### 5.3.3 Guidance Force Versus The Longitudinal Stator Position

In order to evaluate the influence of the longitudinal position of the magnetic way versus the stator, two 3D models are considered (Figure 17). For the first model (Fig. 17.a), the stator tooth is in the axis of the magnetic way pole transition. For the second model (Fig. 17.b), the stator tooth is in the axis of the magnetic way pole. The evolution of the guidance force versus eccentricity is plotted in Figure 18 showing that the situation where the tooth is in the axis of the pole leads to a higher force; the gradient of the force Kz is 12% higher. Indeed, as seen in Figure 17, the spatial repartition of the magnetic flux under the tooth is more homogeneous when the tooth is in the axis of the pole, because the flux leakages between two consecutive permanent magnets are not flowing through the tooth. Consequently, the

flux density is higher and the passive guidance force too.



Case 1
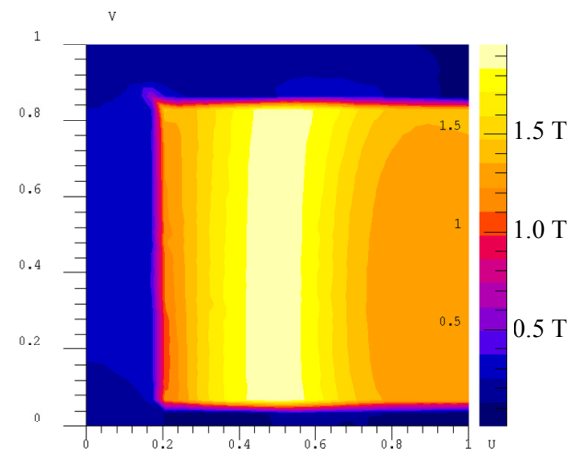
Case 2

Figure 16: 3D FEM - Color shaded of the air-gap flux density
Case 1: Wr = 112 mm; Ws = 90 mm; Air gap = 20 mm
Case 2: Wr = 112 mm; Ws = 90 mm; Air gap = 10 mm
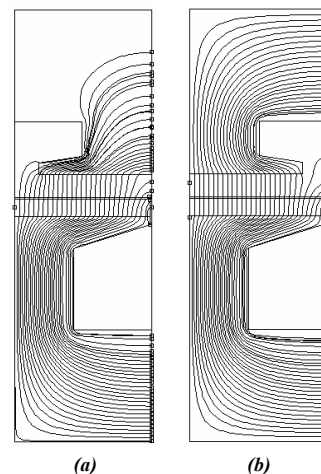Transverse eccentricity Zz = 5.5 mm



(a)          (b)

Figure 17: 3D FEM - Influence of the longitudinal position of the stator tooth
a) the stator tooth is in the axis of the magnetic pole transition;
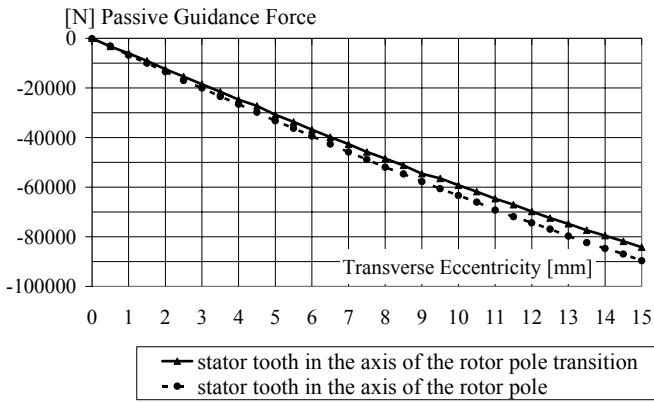b) the stator tooth is in the axis of the magnetic way pole

Figure 18: 3D FEM - Longitudinal position influence on the guidance force
Case: Wr = 112 mm; Ws = 90 mm; Air gap = 20 mm

## 5.4 Design Strategies

The previous analysis permits to define two design strategies. Depending on the required force gradients, these strategies are defined considering Figure 19 results:

- single magnetic way;
- two parallel magnetic ways.

Possible air gap values complete these strategies:

*Case a*: Single magnetic way; Wr = 112 mm; Ws = 90 mm; Air gap = 20 mm;

*Case b*: Two parallel magnetic ways; Wr = 56 mm; Ws = 45 mm; Air gap = 20 mm;

*Case c*: Single magnetic way; Wr = 112 mm; Ws = 90 mm; Air gap = 10 mm;

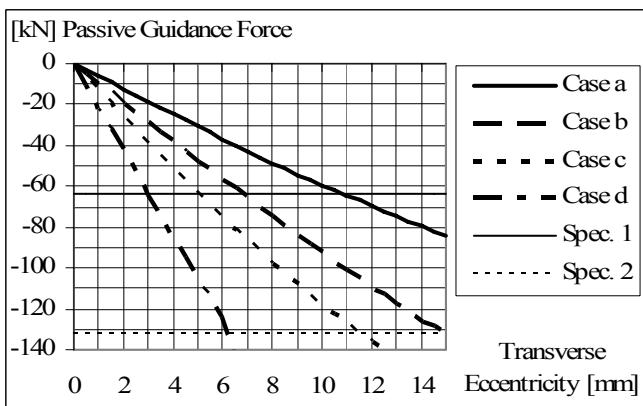*Case d*: Two parallel magnetic ways; Wr = 56 mm; Ws = 45 mm; Air gap = 10 mm.



Figure 19 : Passive guidance force versus transverse offset
Stator tooth is in the axis of the magnetic way pole transition

Table 3: Results corresponding to cases a to d of Figure 19.
Zz1 is determined for a transverse force of 64000 N
Maximum acceleration, energy and power are determined for a variation $\Delta Zz = 5.5$ mm (see Chapter 6)

| Zz1 | Kz | T | $a_{max}$ | $v_{max}$ | $W_{kinetic}$ | $P_{max}$ | Fig. 19 |
|-----|-----|-----|-----|-----|-----|-----|-----|
| mm | MN/m | s | m/s² | m/s | J | W | Cases |
| 11 | -5.88 | 0.73 | 0.403 | 0.05 | 88 | 761 | a |
| 7 | -8.88 | 0.60 | 0.611 | 0.06 | 134 | 1416 | b |
| 5 | -12.74 | 0.50 | 0.876 | 0.07 | 192. | 2432 | c |
| 3 | -20.77 | 0.39 | 1.428 | 0.09 | 314 | 5061 | d |

Figure 20 represents the transverse view of the principle of two magnetic ways. The copper losses of the stator winding and also the copper losses of the pole inductors increase compared to the concept of a single magnetic way.
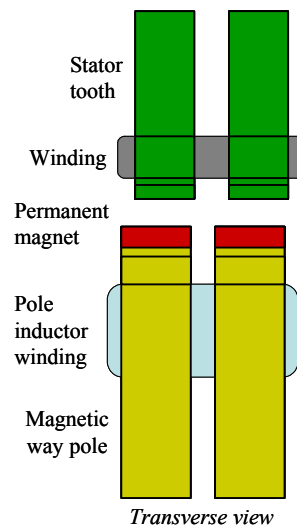


Figure 20: Principle of two parallel magnetic ways

## 6 VEHICLE GUIDANCE DYNAMICS

### 6.1 Involved Forces

The forces involved in the transversal direction are presented hereafter.

- The positioning of the track in space is determined so that the vehicle follows a given ideal trajectory, this trajectory necessitates the occurrence of transversal forces to inscribe the vehicle in the trajectory. Moreover, the passing of a curve with a different speed as the designed one necessitates a transversal force to compensate for acceleration effects as presented in Chapter 2.2. In order to minimize adverse dynamical effects, the trajectories are based on sinusoidal curves.
- The stator assembling in the tunnel have a certain precision, the eccentricity associated with this precision generates a dynamic transversal force depending on the vehicle speed. The variations of the eccentricity along the direction of motion influence the transversal forces. The precision of the measurement[13, 14] based on the principle of

the metrological train is 1 mm over a 25 m distance and 3 mm over a 240 m distance. The adjustment precision at support, associated with the manufacturing precision of the stator, can be kept below 0.4 mm.

• Unsteady aerodynamic forces associated with aerodynamic instabilities occur principally at the vehicle tail. Depending on the geometry of the tail, they are usually of higher amplitude in tunnels, with partial vacuum, than in open air.

## 6.2 Elementary Oscillator

### 6.2.1 Dynamic

To have a first overview of the dynamic behavior of the vehicle versus a variation of the transverse eccentricity, the vehicle is considered as an elementary oscillator. The levitation and the guidance forces being orthogonal, a decoupling of the dynamic behavior permits to give the trends of the system. For the guidance, considering the case of a vehicle moving on a flat plane and for a transverse offset $Zz$, the movement of the vehicle is defined as:

$$m_{total} \cdot \frac{d^2 Zz}{dt^2} = Fx_{guidance} - Fx_{resis\tan t} \qquad [N] \quad (13)$$

Assuming no natural damping and no aerodynamic transverse forces, around the transverse offset $Zz0$, Equation 13 becomes:

$$-m_{total} \cdot \frac{d^2 Zz}{dt^2} + (Zz - Zz0) \cdot Kz = 0 \qquad [N] \quad (14)$$

With:

$$Kz = \left. \frac{dF_{Zz}}{dZz} \right|_{Zz = Zz0} \qquad [N/m] \quad (15)$$

The mechanical pulsation and the time period are:

$$\varpi = \sqrt{\frac{|Kz|}{m_{total}}} \qquad [1/s] \quad (16)$$

$$T = 2 \cdot \pi \cdot \sqrt{\frac{m_{total}}{|Kz|}} = \frac{1}{f_s} \qquad [s] \quad (17)$$

The kinematics of the system based on Equation 14, without damping effect, correspond to:

$$Zz = Zz0 + \Delta Zz \cdot \cos(\varpi \cdot t) \qquad [m] \quad (18)$$

$$\frac{dZz}{dt} = -\Delta Zz \cdot \varpi \cdot \sin(\varpi \cdot t) \qquad [m/s] \quad (19)$$

$$\frac{d^2 Zz}{dt^2} = -\Delta Zz \cdot \varpi^2 \cdot \cos(\varpi \cdot t) \qquad [m/s^2] \quad (20)$$

Where $\Delta Zz$ is the maximum amplitude of the oscillation around the equilibrium position $Zz0$. A transversal perturbation affects the passenger comfort, consequently Equation 14 must satisfy:

$$\Delta Zz \cdot \frac{|Kz|}{m_{total}} \le \sqrt{2} \cdot a_{comfort} \qquad [m/s^2] \quad (21)$$

This situation would happen in reality if the system faces a step corresponding to $\Delta Zz$.

### 6.2.2 Energy Approach

In order to have a damping effect with a passive guidance force, the system must partially absorb the kinetic energy due to a transverse perturbation. The kinetic energy is expressed as:

$$W_{kinetic} = \frac{1}{2} \cdot m_{total} \cdot (\Delta Zz \cdot \varpi)^2 \qquad [J] \quad (22)$$

$$W_{kinetic} = \frac{1}{2} \cdot \Delta Zz \cdot \Delta Zz \cdot |Kz| \qquad [J] \quad (23)$$

The corresponding power is equal to:

$$P(t) = \frac{1}{2} \cdot m_{total} \cdot \Delta Zz^2 \cdot \varpi^3 \cdot \sin(2 \cdot \varpi \cdot t) \qquad [W] \quad (24)$$

With:

$$\left. \begin{array}{l} v_{max} = \Delta Zz \cdot \varpi \\ a_{max} = \Delta Zz \cdot \varpi^2 \\ P_{max} = \frac{1}{2} \cdot m_{total} \cdot \Delta Zz^2 \cdot \varpi^3 \end{array} \right\} \qquad [W] \quad (25)$$

The different corresponding results are given in Tables 2 and 3, for the defined simulated cases.

### 6.2.3 Effect Of A Real Track Profile

Considering the vehicle submitted to forces associated with a deflection of the "real" track trajectory as shown on Figure 21, the profile of the stator can be expressed as:

$$Zz(t) = d \cdot \sin\left(\frac{\pi \cdot v \cdot t}{D_{track}}\right) \qquad [m] \quad (26)$$

The deflection of the force[15] can be expressed as:

$$u(t) = \frac{d}{1 - \left(\frac{\Omega}{\varpi}\right)^2} \cdot \sin(\Omega \cdot t) \qquad [m] \quad (27)$$

With:

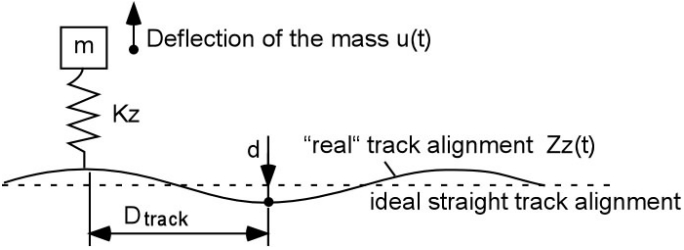$$\Omega = \frac{\pi \cdot v}{D_{track}} \qquad [1/s] \quad (28)$$



Figure 21: Simplified system to simulate the vehicle behavior following a "real" profile Zz of the stator

The maximal value of u ($u_{max}$) depends on the amplitude and wave length of the track alignment accuracy, as well as on the vehicle speed and the dynamic characteristics of the oscillator. Critical conditions are given by the relation:

$$\frac{v}{D_{track}} = \frac{\varpi}{\pi} \qquad [1/s] \quad (29)$$

At the considered speed of 139 m/s, the corresponding value of $D_{track}$ is 50.4 m. The associated value for d using the metrological train is approx. 1.5 mm. At the same speed, the following Table 4 gives typical values for peak displacement $u_{max}$ and the associated peak acceleration $\ddot{u}_{max}$. Table 4 corresponds to the passive guidance force defined by the single magnetic way: case a of Chapter 5.4.

Table 4: Results corresponding to cases a of Figure 19

| $D_{track}$ | d | v | $\omega$ | $\Omega$ | $u_{max}$ | $\ddot{u}_{max}$ |
|---|---|---|---|---|---|---|
| m | m | m/s | 1/s | 1/s | m | m/s$^2$ |
| 5 | $0.4\ 10^{-3}$ | 139 | 8.66 | 87.3 | $3.98\ 10^{-6}$ | 0.03 |
| 25 | $1.0\ 10^{-3}$ | 139 | 8.66 | 17.5 | $3.26\ 10^{-4}$ | 0.10 |
| 240 | $3.0\ 10^{-3}$ | 139 | 8.66 | 1.82 | $3.14\ 10^{-3}$ | 0.01 |

Equation 27 shows the necessity to handle adequately the resonant frequency by adding a damping effect.

## 6.3 Damping Effect

### 6.3.1 Ideal Damping
The ideal value for the viscous damping coefficient is characterized by the following characteristics [15]:

$$c = 2 \cdot \sqrt{m_{total} \cdot Kz} \qquad [Ns/m]$$
$$(30)$$

Nevertheless, half of this value allows keeping the magnification factor of the movement close to 1 and one fourth of this value limits the magnification factor at about 2.

### 6.3.2 Mechanical Damper
A vibratory subsystem (index t) attached to the main oscillator can also be considered to absorb the vibration of the main oscillator (index s), essentially at the resonant frequency, as shown on Figure 22. The optimal frequency of the damper[16] is given by:

$$f_t = f_s \cdot \frac{m_s}{m_s + m_t} \qquad [Hz] \quad (31)$$

In the vehicle, only a few components can be gathered to build such a secondary vibratory system. A preliminary estimation showed that about 4 tons of equipments can be used for this purpose. Therefore the mass ratio will be low (about 0.05) and the frequency of the absorber will be slightly lower (1.31 Hz) than the frequency of the main system (1.38 Hz). This solution allows limiting the magnification factor at the resonance frequency of the main oscillator.
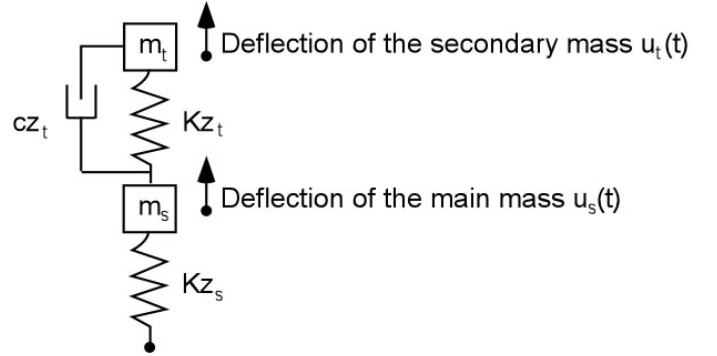


Figure 22: System with a mechanical damper

### 6.3.3 Magnetic Way Iron Losses As Damping Effect
Table 2 indicates that the maximum power is about 2.5 kW. This value should be compared to the iron losses of the magnetic way of 139.6 kW (Table 1) and to the total losses of 203.2 kW, thus to 1.8 % of the magnetic way iron losses or 1.23 % of the total losses.

Such a comparison indicates that the possible magnetic way iron losses induced by the transverse oscillations could be acting as a damper, without affecting dramatically the efficiency of the system. The study of such phenomena requires simulating in 3D FEM, the transient dynamic behavior.

## 6.4 Vehicle At Stalls In A Curve

To maintain the vehicle at stall in a curve of inclination and still to obtain an admissible transverse eccentricity, Figure 19 indicates that the air gap should be reduced in order to produce a transverse force of 134240 N. An air gap of 10 mm should be considered as a limit case.

A possible solution consists to land at a given air gap. In general, it is possible, when the vehicle is stopped, to have a mechanical actuator that pushes the skids to the rail (skids are always necessary in order to handle the fact that levitation system is holonomic). With this system, a prolonged stop can be handled with minimum energy requirement.


# 7 CONCLUSIONS

The combination of the propulsion with the levitation improves the heat transfer under partial vacuum conditions. Such a solution permits long stator section lengths without loosing too much on the complete system efficiency by using permanent magnet for the excitation. This paper is a first order analysis to complete the study by the investigation of the passive guidance forces. The following points can be considered.

- The passive guidance forces are close to a linear function for the admissible range of the transverse eccentricity.
- The dynamic characteristics of the oscillator necessitate the use of an electromechanical or mechanical damping system in order to handle the behavior of the system at the resonance frequency. The dynamic is highly dependant on the speed, the dynamical characteristics of the oscillator and the precision of alignment of the stator in the tunnel. Considering dynamic effects in general, the geometry of the route plays also an important effects on the dynamics of the system.

The following next steps are seen:

- Investigation of the aerodynamic lateral perturbations.
- Complete dynamic analysis of the damping effect due to the iron losses in the magnetic way.

# 8 SPECIFICATIONS

Table 5: Swissmetro specifications: Variants A, B, C and D.

| Swissmetro Variants | | | A | B | C | D |
|---|---|---|---|---|---|---|
| Acceleration | | [m/s$^2$] | 1.3 | 1.3 | 1.3 | 1.3 |
| Speed | | [m/s] | 139 | 139 | 139 | 139 |
| Frequency per direction | | [sec] | 360 | 360 | 360 | 360 |
| Vehicle | Total mass | [ton] | 80 | 80 | 80 | 80 |
| | Total length | [m] | 80 | 80 | 80 | 80 |
| | Number of cells | [-] | 4 | 4 | 4 | 4 |
| | Nose length | [m] | 15 | 15 | 15 | 15 |
| | Tail length | [m] | 15 | 15 | 15 | 15 |
| | Cell length | [m] | 12.5 | 12.5 | 12.5 | 12.5 |
| | Number of passengers | [-] | 200 | 200 | 200 | 200 |
| | Propulsion in nose and tail | | no | no | no | yes |
| Propulsion | Air gap | [m] | 0.02 | 0.02 | 0.02 | 0.02 |
| | Total mechanical power | [MW] | 6 | 6 | 6 | 6 |
| | Mech. power per section | [MW] | 6 | 0.75 | 0.75 | 0.25 |
| | Number of motors per cell | [-] | - | 2 | 2 | 4 |
| | Max. total propulsion force | [kN] | 104 | 104 | 104 | 104 |
| | Design speed | [m/s] | 57.7 | 57.7 | 57.7 | 57.7 |
| | Number of sections per cell | [-] | 2 | 2 | 2 | 2 |
| | Magnetic way section length | [m] | 9.3 | 5.08 2 | 5.08 2 | 10.1 6 |
| | Pole pitch | [m] | 0.32 4 | 0.23 1 | 0.23 1 | 0.23 1 |
| | Number of poles per section | [-] | - | 22 | 22 | 44 |
| Levitation | Air gap | [m] | 0.02 | 0.02 | 0.02 | 0.02 |
| | Number of poles per section | [-] | - | 22 | 22 | 44 |
| | Number of inductors per cell | [-] | 4 | 44 | 44 | 88 |
| | Force per inductor (pole) | [kN] | 33 | 2.97 | 2.97 | 1.49 |
| | Power loss (mean value) | [kW] | 3.3 | 0.4 | 0.4 | |
| | Mass of one inductor (pole) | [kg] | 171 | 56 | 56 | 17 |

**Variant A**: short stators fixed with the tunnel; **Variant B**: stators on board of the vehicle, References [1, 8, 9]
**Variants C**, **D**: long stator fixed with the tunnel, propulsion combined with levitation, References [10, 12]


# 9 LIST OF SYMBOLS

| | | |
|---|---|---|
| B | flux density | [T] |
| D | distance | [m] |
| F | force | [N] |
| Kz | gradient of the force | [N/m] |
| P | power | [W] |
| R | curve radius | [m] |
| T | time period | [s] |
| W | energy | [J] |
| Ws | stator stack width | [m] |
| Wr | magnetic way active width | [m] |
| Zz | transverse offset | [m] |
| | | |
| a | acceleration | [m/s$^2$] |
| c | viscous factor | [Ns/m] |
| d | distance | [m] |
| f | mechanical frequency | [Hz] |

| g | earth acceleration | $[m/s^2]$ |
|---|---|---|
| l | length | [m] |
| m | masse | [kg] |
| t | time | [s] |
| u | length | [m] |
| v | coordinate | [m] |
| x | coordinate | [m] |
| y | coordinate | [m] |
| z | coordinate | [m] |
| Λ | permeance | [H] |
| α | curve plane inclination | [°geom] |
| δ | air gap | [m] |
| ω | pulsation | [1/s] |
| μ | permeability | [Vs/Am] |

## 10 REFERENCES

(1) A. Cassat, M. Jufer, "MAGLEV Projects Technology Aspects and Choices", IEEE Transactions on Applied Superconductivity, Volume 12, Issue 1, March 2002, Page(s): 915 – 925.

(2) S. Miyamamoto, Y. Osada, K. Yamazumi, T. Furuki, "The Status of the Running Tests of JR–Maglev", MAGLEV 2004, October 26-28, 2004, Shanghai, China, Proceedings, pages: 60-64, Vol. I.

(3) U. Henning, D. Hoke, J. Nothhaft, "Development and Operation Results of Transrapid Propulsion System", MAGLEV 2004, October 26-28, 2004, Shanghai, China, Proceedings, pages: 759-780, Vol. II.

(4) Y. Yasuda, M. Fujino, M. Tanaka, S. Ishimoto, "The First HSST Maglev Commercial Train in Japan", MAGLEV 2004, October 26-28, 2004, Shanghai, China, Proceedings, pages: 76-85, Vol. I.

(5) MagneMotion IEE Proceedings-Electric Power Applications Synchronous machine design and manufacturing Number:6,917,136 from the United States Patent and Trademark Office (PTO) owispatent.

(6) R.F. Post, D. D. Ryutov, "The Inductrack: A Simpler Approach to Magnetic Levitation", IEEE Transactions on Applied Superconductivity, 10, 901 2000.

(7) H. Gurol, R. W. Baldi, "General Atomic Test Track Status", LDIA 2005, Linear Drives for Industrial Applications, Proceedings, September 25-28, 2005, pp 251- 253, Kobe-Awaji, Japan.

(8) A. Cassat, "Electromécanique", SWISSMETRO - Main Study - Level B, Swissmetro SA, CP 5278, CH-1211 Genève, May 31, 1999.

(9) A. Cassat, V. Bourquin, M. Mossi, M. Badoux, D. Vernez, M. Jufer, N. Macabrey, P. Rossel, "SWISSMETRO - Project Development Status", International Symposium on Speed-up and Service Technology for Railway and Maglev Systems 2003 (STECH'03). 2003.8. 19-22, pp 453-460, Tokyo, Japan.

(10) A. Cassat, C. Espanet, "SWISSMETRO: Combined Propulsion with Levitation and Guidance", MAGLEV 2004, October 26-28, 2004, Shanghai, China, Proceedings, pages: 747-758, vol. II.

(11) M. Jufer, V. Bourquin, "Développement du projet Swissmetro par une plate-forme numérique", REE Revue de l'Electricité et de l'Electronique-SEE, Paris, No3, mars 2005, pp 97-101.

(12) A. Cassat, C. Espanet, V. Bourquin, P. Hagmann, M. Jufer, "SWISSMETRO - Polarized Linear Motor Combined With Levitation Actuators", LDIA 2005, The Fith International Symposium on Linear Drives for Industry Applications, September 25-28, 2005, pp 247-250, Awaji Yumebutai, Hyogo, Japan.

(13) H. Dupraz, W. Coosemans, F. Ossart, V. Bourquin : "Projet HISTAR – Alignement par écartométrie biaxiale d'une maquette de train à très grande vitesse", Revue XYZ, no 83, p. 65-69, 2000.

(14) H. Dupraz, W. Coosemans, et al. : "High-precision alignment for the HISTAR project", Ingenieurvermessung 2000/K, Schnädelbach, hg. XIII. Int. Course on Engineering Surveying, Verlag K. Wittwer, Stuttgart, 2000.

(15) W. Weaver, S. P. Timoshenko, D. H. Young : "Vibration problems in engineering", 5th edition, John Wiley & Sons, New-York, 1990.

(16) H. Bachmann et al. ; "Vibration problems in engineering", Birkhäuser, Basel, 1995.